Hydrodynamic Coefficient Estimation of Small Autonomous Underwater Vehicle

Gan Zhang, Yinfu Lin, Ji Huang, Lin Hong, and Xin Wang(✉)

Harbin Institute of Technology, Shenzhen, Guangdong, China
wangxinsz@hit.edu.cn

Abstract. Autonomous underwater vehicles (AUVs) have been widely used in many aspects of the underwater world for their autonomy and robust flexibility. However, the dynamic performance of the small AUVs is strongly affected by hydrodynamic effects. In this work, based on a novel designed small AUV, we conduct a hydrodynamic coefficients estimation work by adopting the computational fluid dynamics (CFD) method. Firstly, the resistance to AUV under different propeller layout conditions is analyzed. Secondly, to study the hydrodynamic coefficients of the AUV at different pitch angles, we simulated the movement of the AUV in the Fluent module and determined the thrust of the propeller by estimating the axial and radial forces. Simulation results show that the resistance and sinking force coefficients of the designed AUV are positively correlated with pitch angle and negatively correlated with Reynolds number. This work provides a vital reference for designing effective control strategies for small underwater vehicles.

Keywords: Computational fluid dynamic · Autonomous underwater vehicle · Hydrodynamic coefficients

1 Introduction

Due to the complex underwater environment, the water flow has a great impact on autonomous underwater vehicles. Therefore, in order to control AUVs' motion efficiently and stably, it is necessary to analyze the force conditions and hydrodynamic coefficients of the robot in the underwater intervention process. Nowadays, in the motion simulation of AUV, many research works have been conducted by using CFD methods. In order to study AUV's hydrodynamic effects, Zheng *et al.* [1] used computational fluid dynamic method to analyze the resistance and hydrodynamic coefficients of AUV at different speeds. Some fluid simulations were performed on AUV's external attachments. Wang *et al.* [2] optimized the hydrodynamic performance of AUV with various appendages. The optimization results showed that the influence of attachments on the hydrodynamic performance was proportional to their size, and attachments' distributed layout was beneficial to reduce the resistance. Zhao *et al.* [3] established a motion simulation platform for AUV attachments. Maneuverability of AUV was simulated in horizontal and vertical planes. In order to evaluate the influence of the attachments, the fluid properties of AUV with or without attachments were compared. Julian Hoth *et al.* [4] determined the

X.-J. Liu et al. (Eds.): ICIRA 2021, LNAI 13016, pp. 115–125, 2021.
https://doi.org/10.1007/978-3-030-89092-6_11

flow parameters around AUV. He used different methods to perform CFD simulations on the AUV and analyzed the pressure data. The results showed that the method which used vector machine could produce more accurate results. A. Muthuvel *et al.* [5] used a commercial CFD package called STAR-CCM+ to simulate the flow around AUV with different attachments. Ammar Amory *et al.* [6] used ANSYS Fluent software to simulate fluid properties of a fish-like AUV. Its fluid properties were compared with the torpedo AUV to demonstrate that the fish-like AUV had less resistance when running. Madan A. D *et al.* [7] used semi-empirical formula to analyze the relationship between sizes of AUV and lift and drag forces. Ali Nematollahi *et al.* [8] analyzed the influence of different submergence depths and vehicle speeds on the hydrodynamic performance of underwater vehicles, and summarized some conclusions. Different pitch angles have a great impact on the motion of AUV. A. Mitra *et al.* [9] conducted simulations and experiments on the hull of AUV. He explored the flow characteristics of AUV with different submerged depths and angles of attack. It provided a method to improve the design of AUV. Su *et al.* [10] designed an AUV with vector thruster and calculated the hydrodynamic coefficients of AUV at different angles of attack by CFD software. P. Jagadeesh *et al.* [11] analyzed the hydrodynamic coefficients of the torpedo-type AUV under different pitch angles by both CFD simulation and experiment. The results helped with the design of AUV.

In this paper, Sect. 2 introduces the fluid dynamics model used in fluid simulation and presents the influence of different propeller layouts on resistance coefficient of AUV. Section 3 analyzes resistances and sinking forces of AUV with different pitch angles and Reynolds numbers. Finally, the conclusion of this article is in the Sect. 4.

2 Fluid Dynamics Model

In this work, three assumptions are made in the process of our CFD simulation: (1) A fixed-size cuboid is used as the simulation area, and its boundary effect is ignored for simulating an infinite AUV working area. (2) We take the resistance in still water into consideration but ignore the influence of currents, since this AUV only works in lakes and rivers. (3) The torques generated by their rotation can cancel each other due to the symmetrical placement of propellers. Meanwhile, the thrust is considered.

2.1 Fluid Flow Model

Before establishing computational model, Reynolds number can be determined as follows:

$$\mathrm{Re} = \frac{\rho u L}{\mu} \tag{1}$$

where the density of water ρ equals 998.2 kg/m^3, dynamic viscosity coefficient μ equals 1.003 * 10^{-3}kg/m·s, the effective length of AUVL equals 0.2 m, and u is the velocity of AUV.

When the AUV travels at the speed of 0.1 m/s, the Reynolds number is 1.99 * 10^4, so it should be considered as a turbulence model. However, the analysis of turbulent

flow field is very complicated. There may be eddy currents of different sizes interfering with each other, which makes the simulation more difficult. Here, we choose standard k-epsilon model to simulate AUV's movement. It is a common turbulence model, which can be used to solve the external flow problem of complex geometry. It can be described as follows:

$$\frac{\partial(\rho k)}{\partial t} + \frac{\partial(\rho k u_i)}{\partial x_i} = \frac{\partial}{\partial x_j}[(\mu + \frac{\mu_t}{\sigma_k})\frac{\partial k}{\partial x_j}] + G_k + G_b - \rho\varepsilon - Y_M + S_k \quad (2)$$

$$\frac{\partial(\rho\varepsilon)}{\partial t} + \frac{\partial(\rho\varepsilon u_i)}{\partial x_i} = \frac{\partial}{\partial x_j}[(\mu + \frac{\mu_t}{\sigma_\varepsilon})\frac{\partial \varepsilon}{\partial x_j}] + C_{1\varepsilon}\frac{\varepsilon}{k}(G_k + C_{3\varepsilon}G_b) - C_{2\varepsilon}\rho\frac{\varepsilon^2}{k} + S_\varepsilon \quad (3)$$

where k is kinetic energy, ε is turbulent dissipation rate, α is turbulent Prandtl number, G_k and G_ε are kinetic energy changes caused by velocity gradient and buoyancy, Y_M is fluctuations caused by transitional diffusion in compressible turbulence, C is empirical coefficient, S is custom constant.

2.2 3D Modeling and Meshing

We design a small AUV with flexibility and portability, which can work in lakes and rivers. When AUV is working underwater, different layouts of propellers may have different effects on the resistance. In this section, the influence of propeller layout on its resistance is analyzed through CFD simulation. The 3D models of AUV with different propeller layouts are shown in Fig. 1.

(a) (b) (c)

Fig. 1. 3D models of AUV. (a) AUV with no propeller. (b) AUV with external propellers. (c) AUV with internal propellers.

Due to the small size of AUV, it is meshed with the highest-quality unstructured grid in ANSYS software, which is a good way to improve the accuracy of the simulation. The finite element models after meshing are shown in Fig. 2.

We use a $20D$*$10D$*$10D$ cuboid as the computational domain where D is the diameter of AUV ($D = 160$ mm). The computational domain after meshing and its boundary conditions are shown in Fig. 3. The whole computational domain including AUV is symmetrical about the middle plane, so half of the domain is used to improve the calculation efficiency. During the simulation, AUV is static and different speeds of water are used to simulate different forward speeds of AUV.

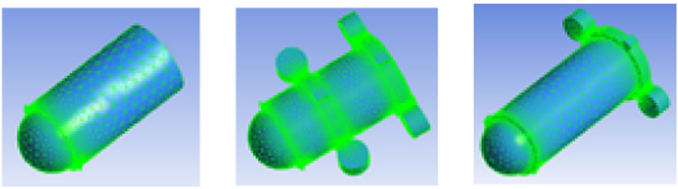

(a) (b) (c)

Fig. 2. AUV after meshing. (a) AUV with no propeller. (b) AUV with external propellers. (c) AUV with internal propellers.

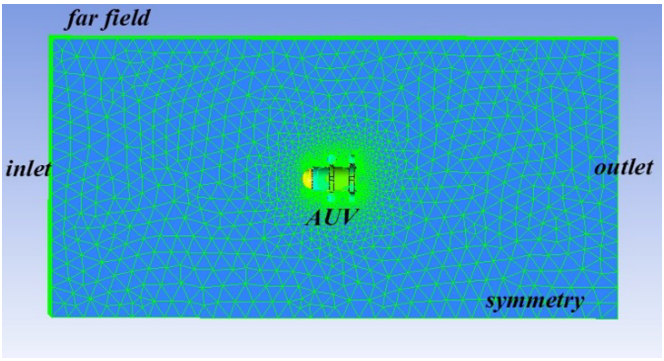

Fig. 3. Computational domain and boundary conditions.

2.3 Calculation Results

AUV is set to travels at the speed of 0.6 m/s in water. As shown in the following equation, the resistance to AUV can be calculated:

$$F_D = 0.5\rho C_D v^2 A \tag{4}$$

where C_D denotes the resistance coefficient, F_D denotes the resistance, v denotes the speed of AUV, ρ denotes the density of the fluid, and A denotes the cross-sectional area. The resistance coefficients and resistances are shown in Table 1.

From Table 1, we can find that AUV without propeller has the least resistance when running in water. After AUV is equipped with external propellers or internal propellers, its resistance will double. However, the difference between them is small. It can be clearly seen that their efficiency of underwater motion is similar. For the convenience of control, AUV with external propellers is used for the following simulation experiment.

3 Simulation Experiment

AUVs with different pitch angles will be subjected to different forces from water flow. The forces on AUV are calculated by CFD software, and they are analyzed to obtain the hydrodynamic coefficients as well as axial and radial forces of AUV.

Table 1. Resistance coefficients and resistances to AUV.

Propeller layout	Cross-sectional area	Resistance coefficient	Resistance
No propeller	0.0064π	0.5523	1.9989N
Internal propellers	0.01π	0.6796	3.8431N
External propellers	0.01π	0.7227	4.0870N

3.1 Initial Conditions and Force Analysis

The length-diameter ratio (L/D) of this AUV is 2.1875, and Table 2 shows the initial conditions of the simulation.

Table 2. Initial conditions.

Parameter	Unit	Numerical description
Reynolds number	($\times 10^5$)	0.4, 0.8, 1.2, 1.6, 2.0
Pitch angle (α)	°	0, 5, 10, 15, 20
Hydrodynamic coefficient	--	Resistance and sinking force

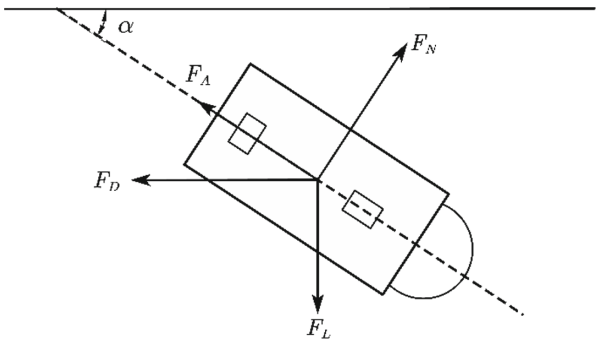

Fig. 4. Force analysis of AUV.

As shown in Fig. 4, F_L denotes the sinking force, F_D denotes the resistance, F_A denotes the axial force, F_N denotes the radial force, and α denotes the pitch angle. The relationship among them can be described as follows:

$$\begin{cases} F_A = F_D \cos\alpha - F_L \sin\alpha \\ F_N = -F_D \sin\alpha - F_L \cos\alpha \end{cases} \tag{5}$$

According to Eq. (4), we can obtain the resistance and sinking force coefficient:

$$C_D = F_D/(0.5\rho v^2 A) \tag{6}$$

$$C_L = F_L/(0.5\rho v^2 A) \tag{7}$$

3.2 Analysis of Simulation Results

When the AUV is moving at different speeds and pitch angles, the resistance and sinking force can be simulated. Simulation results are shown in Table 3 and Table 4.

Table 3. Resistances to AUV with different Reynolds numbers and pitch angles.

Pitch angles	Reynolds numbers ($\times 10^5$)				
	0.4	0.8	1.2	1.6	2.0
0°	0.46N	1.82N	4.08N	7.22N	11.16N
5°	0.51N	2.02N	4.53N	7.96N	12.33N
10°	0.56N	2.18N	4.88N	8.64N	13.45N
15°	0.66N	2.64N	5.91N	10.48N	16.18N
20°	0.73N	2.91N	6.46N	11.47N	17.84N

Table 4. Sinking forces of AUV with different Reynolds numbers and pitch angles.

Pitch angles	Reynolds numbers ($\times 10^5$)				
	0.4	0.8	1.2	1.6	2.0
5°	0.08N	0.30N	0.65N	1.15N	1.61N
10°	0.12N	0.45N	0.98N	1.67N	2.52N
15°	0.16N	0.62N	1.32N	2.25N	3.39N
20°	0.23N	0.88N	1.92N	3.25N	4.87N

After visualizing the data, the resistance and sinking force diagrams are shown in Fig. 5 and Fig. 6.

From Fig. 5 and Fig. 6, it is clearly that resistance and sinking force both have a quadratic relationship with Reynolds number. This result is consistent with Eq. (6) and Eq. (7). Meanwhile, the resistance and sinking force are positively correlated to the pitch angle.

Based on the estimated force, the resistance coefficients and the sinking force coefficients can be calculated separately through Eq. (6) and Eq. (7), as shown in Table 5 and Table 6.

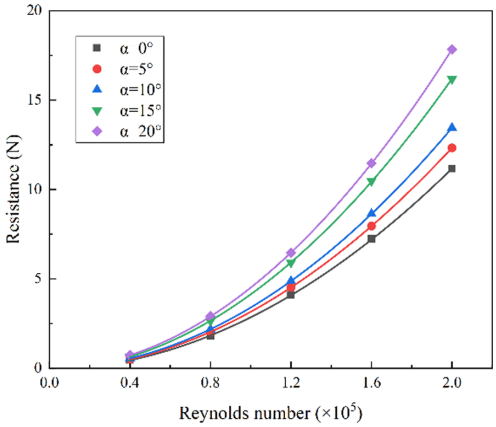

Fig. 5. Resistances to AUV with different Reynolds numbers and pitch angles.

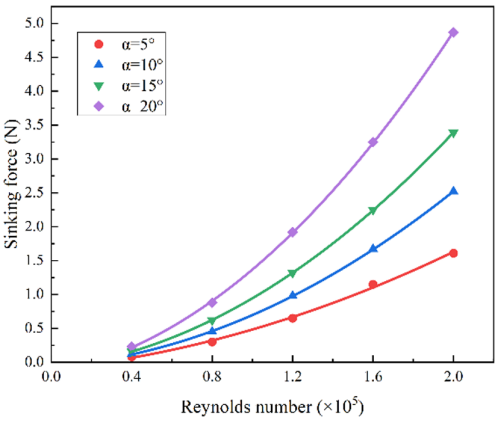

Fig. 6. Sinking forces of AUV with different Reynolds numbers and pitch angles.

Table 5. Resistance coefficients of AUV with different Reynolds numbers and pitch angles.

Pitch angles	Reynolds numbers ($\times 10^5$)				
	0.4	0.8	1.2	1.6	2.0
0°	0.731	0.723	0.722	0.717	0.711
5°	0.814	0.805	0.800	0.792	0.784
10°	0.888	0.868	0.863	0.859	0.857
15°	1.056	1.049	1.045	1.040	1.030
20°	1.172	1.157	1.143	1.141	1.136

Table 6. Sinking force coefficients of AUV with different Reynolds numbers and pitch angles.

Pitch angles	Reynolds numbers ($\times 10^5$)				
	0.4	0.8	1.2	1.6	2.0
5°	0.131	0.121	0.116	0.114	0.102
10°	0.186	0.179	0.173	0.166	0.160
15°	0.258	0.245	0.234	0.223	0.216
20°	0.364	0.349	0.339	0.323	0.310

The resistance and sinking force coefficients diagrams of AUV are shown in Fig. 7 and Fig. 8. When the Reynolds number is constant, the larger the pitch angle is, the greater the resistance coefficient and sinking force coefficient become. It is because the contact area between AUV and the incoming flow increases. When the pitch angle is constant and the Reynolds number increases, the resistance coefficient and sinking force coefficient tend to be smaller. This is because the resistance coefficient includes the pressure coefficient and the viscous coefficient. The pressure coefficient decreases with the increase of Reynolds number, but the viscous coefficient is almost unchanged. When the pitch angle is 0° and the Reynolds number increases, the relationship among the resistance, pressure force and viscous force is shown in Fig. 9.

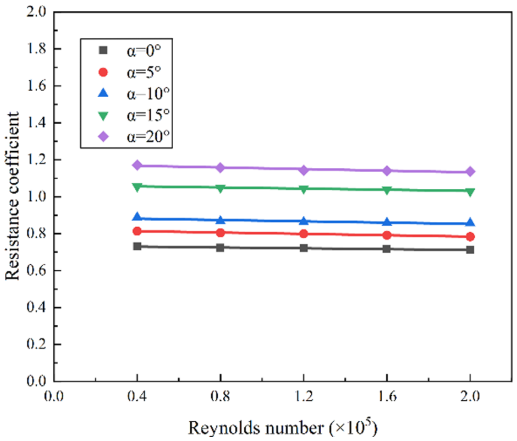

Fig. 7. Resistance coefficients of AUV with different Reynolds numbers and pitch angles.

To obtain the thrust of propellers, we convert the resistance and sinking force into axial and radial forces with Eq. (5). The axial and radial forces can be offset by the thrust generated by the horizontal propellers and the vertical propellers. It provides data reference for controlling the thrust when AUV is moving at different pitch angles. The axial and radial forces of AUV are shown in Table 7 and Table 8 respectively.

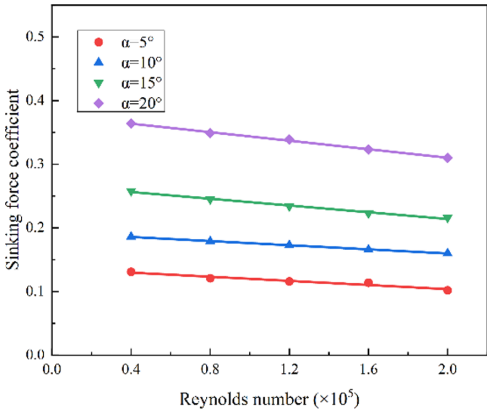

Fig. 8. Sinking force coefficients of AUV with different Reynolds numbers and pitch angles.

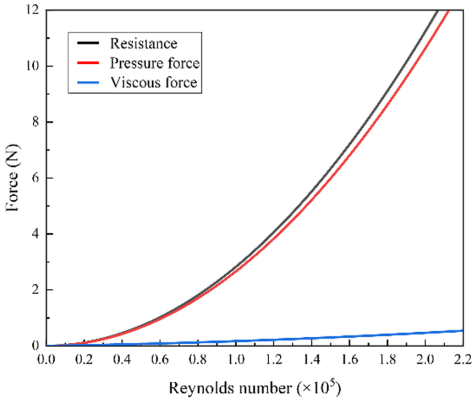

Fig. 9. Relationship between resistance, pressure force, and viscous force.

Table 7. Axial forces of AUV.

Pitch angles	Reynolds numbers ($\times 10^5$)				
	0.4	0.8	1.2	1.6	2.0
0°	0.46N	0.82N	4.08N	7.22N	11.16N
5°	0.50N	1.99N	4.45N	7.83N	12.15N
10°	0.53N	2.07N	4.64N	8.22N	12.81N
15°	0.60N	2.39N	5.37N	9.55N	14.75N
20°	0.61N	2.43N	5.42N	9.67N	15.10N

Table 8. Radial forces of AUV.

Pitch angles	Reynolds numbers ($\times 10^5$)				
	0.4	0.8	1.2	1.6	2.0
0°	0N	0N	0N	0N	0N
5°	−0.13N	−0.48N	−1.05N	−1.84N	−2.68N
10°	−0.21N	−0.82N	−1.81N	−3.15N	−4.82N
15°	−0.33N	−1.28N	−2.80N	−4.88N	−7.46N
20°	−0.47N	−1.82N	−4.01N	−6.97N	−10.68N

4 Conclusion

In this paper, we apply CFD method to estimate the hydrodynamic coefficients and axial and radial forces of a small AUV. Firstly, we establish a simulation model of the designed AUV with Fluent and analyze the resistances to AUV under different propeller layouts and decide to choose AUV with external propellers. Next, hydrodynamic coefficients of AUV moving in different pitch angles are given by simulation. And we discuss the influence of the Reynolds number and pitch angle on hydrodynamic coefficients. The results show that the resistance and sinking force coefficients of AUV will increase with the increase of the pitch angle and decrease with the increase of Reynolds number. Finally, the axial and radial forces of AUV are calculated, which provides data reference for stability control of AUV. In the future, we plan to verify the effectiveness of the fluid dynamic model by field experiments.

Acknowledgment. This work was supported in part by the R \& D plan of key areas in Guangdong Province (No.2019B090920001), and Shenzhen Bureau of Science Technology and Information of China (No.JCYJ20180306172134024).

References

1. Zheng, H., Wang, X., Xu, Z.: Study on hydrodynamic performance and CFD simulation of AUV. In: 2017 IEEE International Conference on Information and Automation. ICIA (2017)
2. Wang, Y., Gao, T., Pang, Y., et al.: Investigation and optimization of appendage influence on the hydrodynamic performance of AUVs. J. Mar. Sci. Technol. **24**, 297–305 (2019)
3. Zhao, J., Su, Y., Ju, L., et al.: Hydrodynamic performance calculation and motion simulation of an AUV with appendages. In: Proceedings of 2011 International Conference on Electronic & Mechanical Engineering and Information Technology, pp. 657–660 (2011)
4. Hoth, J., Kowalczyk, W.: Determination of flow parameters of a water flow around an AUV body. Robotics **8**(1), 5 (2019)
5. Muthuvel, A., Babu, M., Purandarraj, S., et al.: Numerical simulation of flow over an autonomous underwater vehicle with appendages for various turbulence models. In: AIP Conference Proceedings 2039, p. 020038 (2018)
6. Amory, A., Maehle, E.: Modelling and CFD simulation of a micro autonomous underwater vehicle SEMBIO. In: OCEANS 2018 MTS/IEEE Charleston, pp. 1–6 (2018)

7. Madan, A.D., Issac, M.T.: Hydrodynamic analysis of AUV hulls using semi-empirical and CFD approach. Univ. J. Mech. Eng. **5**(5), 137–143 (2017)
8. Nematollahi, A., Dadvand, A., Dawoodian, M.: An axisymmetric underwater vehicle-free surface interaction: a numerical study. Ocean Eng. **96**(mar.1), 205–214 (2015)
9. Mitra, A., Panda, P., Warrior, H.V.: The effects of free stream turbulence on the hydrodynamic characteristics of an AUV hull form. Ocean Eng. **174**, 148–158 (2019)
10. Su, H., Chen, C., Cai, Q., et al.: Computational fluid dynamics study of autonomous underwater vehicle with vectorial thrusters. In: 2018 OCEANS - MTS/IEEE Kobe Techno-Oceans (OTO), pp. 1–5 (2018)
11. Jagadeesh, P., Murali, K., Idichandy, V.G.: Experimental investigation of hydrodynamic force coefficients over AUV hull form. Ocean Eng. **36**(1), 113–118 (2009)